HAL
open science

Correction for Photobleaching in Dynamic Fluorescence Microscopy: Application in the Assessment of Pharmacokinetic Parameters in Ultrasound-Mediated Drug Delivery

Marc Derieppe, Clemens Bos, M. de Greef, Chrit Moonen, Baudouin Denis de Senneville

To cite this version:

Marc Derieppe, Clemens Bos, M. de Greef, Chrit Moonen, Baudouin Denis de Senneville. Correction for Photobleaching in Dynamic Fluorescence Microscopy: Application in the Assessment of Pharmacokinetic Parameters in Ultrasound-Mediated Drug Delivery. Physics in Medicine and Biology, 2015, 61 (2), pp.588. hal-01259337

HAL Id: hal-01259337

https://hal.science/hal-01259337

Submitted on 20 Jan 2016

HAL is a multi-disciplinary open access archive for the deposit and dissemination of scientific research documents, whether they are published or not. The documents may come from teaching and research institutions in France or abroad, or from public or private research centers.

L'archive ouverte pluridisciplinaire **HAL**, est destinée au dépôt et à la diffusion de documents scientifiques de niveau recherche, publiés ou non, émanant des établissements d'enseignement et de recherche français ou étrangers, des laboratoires publics ou privés.

Correction for Photobleaching in Dynamic Fluorescence Microscopy: Application in the Assessment of Pharmacokinetic Parameters in Ultrasound-Mediated Drug Delivery

Short title used as a running head:

Correction for Photobleaching in Ultrasound-Mediated Drug Delivery

M Derieppe[1*], C Bos[1], M de Greef[1], C Moonen[1], and B Denis de Senneville[1,2]

[1]Imaging Division, University Medical Center Utrecht, Utrecht, Netherlands

[2]Institut de Mathématiques de Bordeaux, UMR 5251, CNRS, Université de Bordeaux, Bordeaux, France

Manuscript category: Original article

* Corresponding author

Email: Marc Derieppe - marc.derieppe@gmail.com – tel : +31 (0)6 39 11 74 24

Abstract

Purpose. We have previously demonstrated the feasibility of monitoring ultrasound-mediated uptake of a hydrophilic model drug in real time with dynamic confocal fluorescence microscopy. In this study, we evaluate and correct the impact of photobleaching to improve the accuracy of pharmacokinetic parameter estimates.

Procedures. To model photobleaching of the fluorescent model drug SYTOX Green, a photobleaching process was added to the current two-compartment model describing cell uptake. After collection of the uptake profile, a second acquisition was performed when SYTOX Green was equilibrated, to evaluate the photobleaching rate experimentally.

Results. Photobleaching rates up to 5.0 10^{-3} s^{-1} were measured when applying power densities up to 0.2 $W.cm^{-2}$. By applying the three-compartment model, the model drug uptake rate of 6.0 10^{-3} s^{-1} was measured independent of the applied laser power.

Conclusions. The impact of photobleaching on uptake rate estimates measured by dynamic fluorescence microscopy was evaluated. Subsequent compensation improved the accuracy of pharmacokinetic parameter estimates in the cell population subjected to sonopermeabilization.

Keywords: drug delivery, pharmacokinetic parameters, photobleaching, ultrasound bioeffects, dynamic fluorescence microscopy.

Introduction

Local drug delivery in oncology aims at increasing the dose of an anticancer agent at the tumour site while limiting its concentration in the general circulation [1-2]. Efficient delivery remains challenging owing to the existence of biological barriers, such as the endothelial barrier and tumor-cell plasma membranes for agents that need to reach the intracellular compartment to induce its cytotoxic effect. To increase the permeability of these biological barriers towards compounds exhibiting a low lipophilicity, strategies exploiting acoustic cavitation generated by ultrasound waves (US) have been devised in a localized and non-ionizing fashion [3-7]. Injected intravenously, these gas-filled micrometric particles remain located in the vasculature and induce permeability of the endothelial cells, thus facilitating drug extravasation of therapeutic agents that exhibit poor transendothelial transport. Monitoring of these processes *in vitro* at the cellular level and *in vivo* at the endothelial-barrier level is of special interest to optimize US-mediated delivery protocols and gain insight in US bioeffects.

For this purpose, fluorescence microscopy provides a spatial resolution suitable for cell imaging, and a wide range of fluorescent probes is available to observe mechanisms selectively. As an example, the use of cell-impermeable fluorophores demonstrating a fluorescence signal enhancement when bound to DNA was reported; these fluorophores serve as “smart sensors” for the investigation of US- and microbubble-mediated plasma membrane permeabilization [8]. With a molecular weight close to that of anticancer agents, these fluorophores, *e.g.* SYTOX Green, 600 Da or TO-PRO-3, 671 Da, can be considered models for low molecular weight anticancer drugs.

Capable of collecting images with a high temporal resolution, modern fluorescence microscopy systems paved the way for a broad spectrum of applications providing insights in the spatiotemporal dynamics of biological systems [9-10]. For instance, fluorescence imaging of molecular motors in the cytoplasm [11-12] allowed collecting speed and trajectory estimates, and could relate them to biological conditions. Unfortunately, direct investigation of the fluorescence signal in intensity-based fluorescence microscopy remains challenging due to photobleaching (PB).

PB stems from the photon-induced chemical destruction of a fluorescent molecule that is subjected to excitation light, resulting in the irreversible reduction of fluorescence signal intensity

[13]. Well-described in homogeneous solutions with a controlled chemical environment [14], the PB process remains difficult to assess in biological systems where fluorophores are exposed to a multimolecular chemical microenvironment. This limits systematic quantitative analysis of fluorescence signal intensity data. Even if a number of studies showed that PB is not a fully mono-exponential process [14-16], it is commonly assumed that a single-exponential process describes PB in good approximation [17].

In our previous studies, we demonstrated *in vitro* the feasibility to monitor in real-time the US- and microbubble-mediated permeabilization of a SYTOX Green model drug using a fibered confocal fluorescence microscopy (FCFM) system that avoids the geometrical constraints of standard microscope setups. Having real-time data available should permit to characterize the model drug uptake quantitatively in terms of the uptake kinetics [18]. Thus, we implemented an automated post-processing pipeline to assess the pharmacokinetic parameters of this model drug, including the detection of cells, cell-tracking over the full sequence, and statistical analyses of the cell population in the field of view [19]. However, assessment of pharmacokinetic parameters was hindered by PB inherent of dynamic fluorescence microscopy. In this article, we assess the impact of PB on the observed pharmacokinetic parameters, and evaluate the use of three-compartment models, that include a rate constant to reflect PB.

Materials and Methods

Setup and Experimental Protocol

In this study, dynamic fluorescence data during and after sonoporation were acquired using the protocol presented in Derieppe *et al.* [18]. Briefly, the *in vitro* setup comprised a 37°C water bath containing a 1.5 MHz unfocused mono-element transducer (diameter 20 mm) with the following US settings: 0.9 MPa peak-to-peak pressure, 10 % duty cycle, 1 kHz pulse repetition frequency, 5 s exposure time. These US settings do not induce any temperature rise.

Three days prior to the experiment, 500,000 C6 rat glioma cells were seeded in a 10 mL cell culture chamber (OptiCell™, Thermo Fischer Scientific, Rochester, NY, USA) that is ultrasound and

optically compatible. On the day of experiment, cells were at 90 % confluence. A commercially available ultrasound contrast agent (SonoVue®, Bracco, Milan, Italy) was added to the cells at a 20 microbubble-to-cell ratio; this microbubble density was chosen to optimize the uptake yield, *i.e.*, the highest percentage of cells taking up the dye, while keeping a high cell viability (data not shown). Ten seconds after starting the recording, the cell monolayer was exposed to US waves for 5 s. Making contact with the upper wall of the culture chamber, the tip of the FCFM microprobe (Z-probe - Cellvizio® Dual Band, Mauna Kea Technologies, Paris, France) allowed monitoring the uptake of SYTOX Green fluorescent dye (excitation/emission = 504/523 nm, molecular weight = 600 Da) by means of the fluorescence signal intensity. To evaluate the impact of PB, the experiment was conducted using 0.5 mW, 1.0 mW and 1.6 mW of laser power, which are 25 %, 50 % and 75 % of the maximum laser power, respectively. The lower light intensity was chosen to detect cells first on lower signal-to-noise-ratio images at the early stage of the ultrasound- and microbubble-mediated cell uptake.

Signal Acquisition and Cell Tracking

To monitor US- and microbubble-mediated cell uptake, the fluorescence signal time curve for each individual cell was obtained at a frame rate of 8.5 Hz, *i.e.* the lowest allowed by the FCFM hardware, as described in Derieppe *et al.* [19]. Image analysis was conducted using MATLAB® 2013 (MathWorks, USA). Briefly, a first series of 6 minutes (min) was acquired during which cells were sonicated for 5 s, ten seconds after the acquisition was started (figure 1a). In these images, detection of the cell nuclei was performed using a non-local means approach followed by an intensity threshold for nucleus delineation. The nuclei were then labelled in each frame and automatically tracked over the time series using the iterative closest point method [20] applied between successive images, which is justified since the acquisition frame rate is high compared to the cell motion. Although the fluorescence signal is only collected in the cell nucleus, in the following, it will be thus referred to as the “cell signal”.

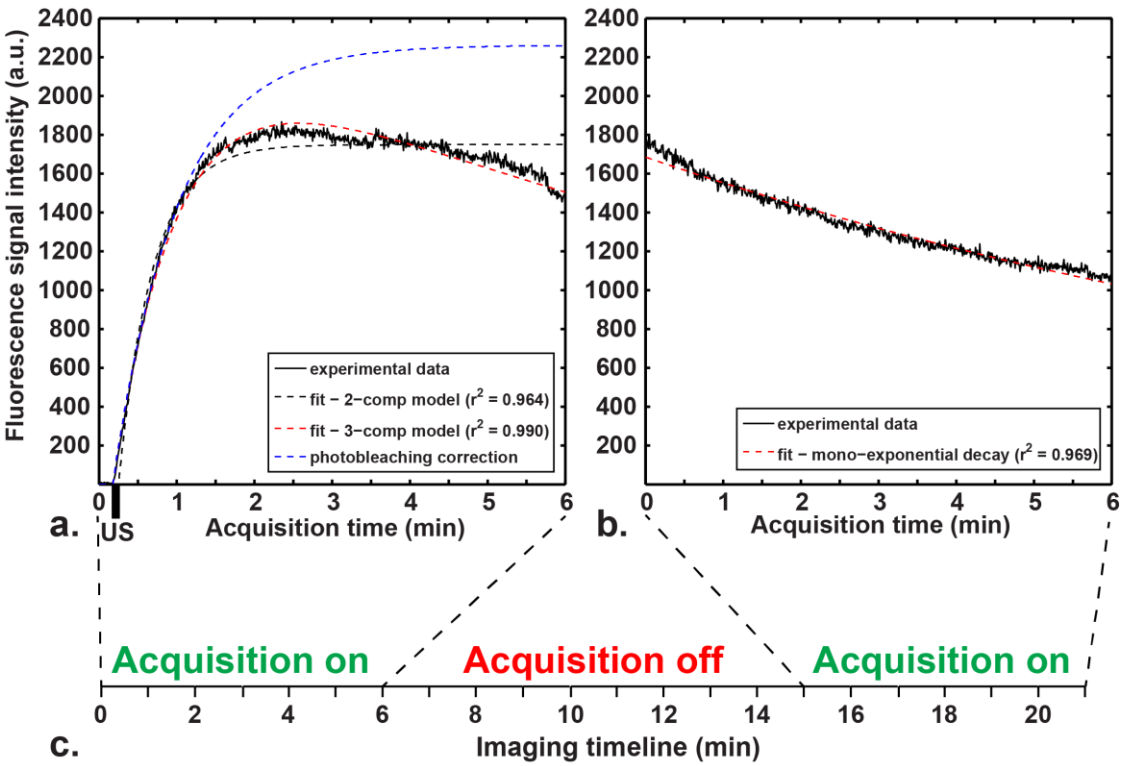

Figure 1. Imaging timeline (c) with a representative fluorescence signal profile of the uptake (a) and the PB (b). A 9-minute interruption allowed waiting for fluorophore equilibration to evaluate PB with the second acquisition (b).

Evaluation of PB was carried out for the same field of view by acquiring a second sequence after the fluorescence signal further equilibrated (figure 1b). Pilot experiments allowed measuring uptake time constants in the range of 3 minutes (two-compartment model). Assuming that the equilibration is reached five times later than the characteristic uptake time constants, equilibration for most cells was sufficiently achieved 15 minutes after US exposure (figure 1c) when a second series was started in which the fluorescence signal decay observed originates from PB (figure 1b).

Mathematical Models and Computation of the Kinetic Parameters

As suggested before [18], the uptake of the model drug in the first image series can be described as a two-compartment model with an extracellular compartment, which initially contains all SYTOX Green molecules, and an intracellular compartment, taking up the model drug during and after US- and

microbubble-mediated sonopermeabilization. After binding to DNA, SYTOX Green fluorescence intensity increases by two orders of magnitude, thus reflecting cell uptake of SYTOX Green. Thus, for the two-compartment model, the time dependence of the fluorescence signal intensity is as follows:

$$I(t) = I_{\infty}[1 - e^{-k_{up}(t-T)}] \quad (1)$$

where I_{∞} is the asymptotic signal enhancement, T the time of fluorescence signal onset, and k_{up} the uptake rate.

In the second image series, PB was evaluated by fitting the fluorescence intensity profiles with a mono-exponential decay, as suggested in the literature [17,21]:

$$I(t) = I_0\, e^{-k_{pb}\, t} \quad (2)$$

where I_0 is the fluorescence signal at the onset of the acquisition, and k_{pb} the PB rate. This model will be named "PB model" in this study.

To take PB into account during the uptake phase when fluorescence signal increases, a three-compartment model can be used where we add an efflux rate of fluorophore molecules subjected to the irreversible damage of PB. The time dependence of the fluorescence signal intensity is then given by:

$$I(t) = I_{\infty} \times \frac{k_{up}}{k_{up} - k_{pb}}[e^{-k_{pb}(t-T)} - e^{-k_{up}(t-T)}] \quad (3)$$

where I_{∞} is the asymptotic fluorescence signal, T the time of fluorescence signal onset, k_{up} the uptake rate, and k_{pb} the PB rate.

The uptake rates and the PB rates were computed using a Levenberg-Marquardt least-squares fit applied to the fluorescence intensity in each individual cell. The model was considered a good description of the enhancement when the goodness of the fit as evaluated by the Pearson's correlation coefficient (r^2) was greater than 0.95.

Abbreviated 2CM in this study, the application of the two-compartment model consisted of fitting the uptake signal profiles of the individual cells with I_{∞}, T and k_{up} as free fit parameters using the signal equation as given by Equation 1. The three-compartment model (Eq. 3) was applied on the uptake signal profile by considering two approaches. First, using the PB model on the data from the equilibrium phase, the PB rate was evaluated in each individual cell experimentally (figure 1b). For each cell, this PB rate then served as an input for a fit of the data to the three-compartment model (Eq.

3), keeping it fixed, while including I_∞, T and k_{up} as fit parameters. Abbreviated $3CM_{ref}$, this model is the reference method in this study. Second, the three-compartment model was used to fit the data of the uptake phase directly, with all the parameters free in the fit ($3CM_{all}$).

Influence of the Acquisition Time - Sensitivity of the Three-compartment Model

Sensitivity of the three-compartment model was evaluated, in particular the influence of errors in determining k_{pb} on the estimation of k_{up}. The estimated uptake rate was noted $\hat{k}_{up}$. To this end, a synthetic uptake signal profile was generated with an asymptotic signal set to 1000 arbitrary units (a.u.), a signal onset at 10 s, a chosen uptake rate k_{up} and a PB rate k_{pb}. Then, the sensitivity of $\hat{k}_{up}$, as determined by fitting of the signal profile with 3CM, to deviations from the chosen PB rate was investigated. This was evaluated by each time generating a randomly perturbed PB rate from a Gaussian distribution centered at the true value of k_{pb}, with a standard deviation of 25 % k_{pb}. The sensitivity was evaluated in a range of PB rates (at 25 %, 50 % and 75 % of laser power) and uptake rates found experimentally, *i.e.* from 0.1 10^{-3} s^{-1} to 3.5 10^{-3} s^{-1}, and from 4.0 10^{-3} s^{-1} to 50.0 10^{-3} s^{-1}, respectively. The simulation was performed using 3 min, 6 min and 9 min of acquisition time for the collection of the uptake profile. For each set of kinetic parameters, the model sensitivity was estimated by assessing the normalized error, defined as the difference of the median value of the estimates $\hat{k}_{up}$ and the chosen k_{up}, divided by the chosen k_{up}, and the normalized precision, *i.e.* the interquartile range of $\hat{k}_{up}$ divided by k_{up}.

Comparison of the methods

For each of the three laser powers, the uptake rate estimates obtained from the 2CM (Eq. 1) and the $3CM_{all}$ (Eq. 1) were compared to the $3CM_{ref}$ by using a Bland-Altman plot representing the difference of the same estimate measured with 2 different methods as a function of their average value [22-23]. The 2CM was compared to the $3CM_{ref}$ by determining the line of best fit with a first-order model as described in Ludbrook et. al. 2010 [24]. The heteroscedasticity was represented by V-shaped standard-deviation lines that were drawn by fitting linearly the absolute values of the residuals, *i.e.* the

differences of the observed values by the predicted ones, against the average values [24]. The resulting coefficients for regression were adjusted by multiplying them by $\sqrt{(\pi/2)}$. It yields increasing standard-deviation values when the average values increase.

Statistical Analysis

Data are presented as median (interquartile range). Statistics have been conducted using GraphPad Prism® software (San Diego, CA, USA). PB rates evaluated experimentally at 25 %, 50 % and 75 % of laser power were compared one-by-one using the unpaired non-parametric Mann-Whitney test (MW) (figure 3). Uptake rates as well as the PB rates obtained using the different models at different laser powers were compared using Wilcoxon's paired signed rank test (WX). The results were considered significant when the p-value (p) was lower than 0.05.

Results

Real-Time Imaging of Model Drug Uptake and Experimental Evaluation of Photobleaching

The first 6-minute acquisition shows that exposure of the cells to US waves leads to a fluorescence signal enhancement that starts at the onset of US, and continues after the end of US exposure (figure 1a, Fig. 2a-d), as was described previously by Derieppe *et. al.* 2013 [18]. Then, after the SYTOX Green model drug had further equilibrated, the PB profile was acquired in the same field of view (figure 1b, Fig. 2e-h). The fluorescence signal at 15 minutes (figure 1b) was higher than that at 6 minutes (figure 1a), owing to influx of fluorophores in the cell nuclei binding to DNA, spared from PB between 6 minutes and 15 minutes.

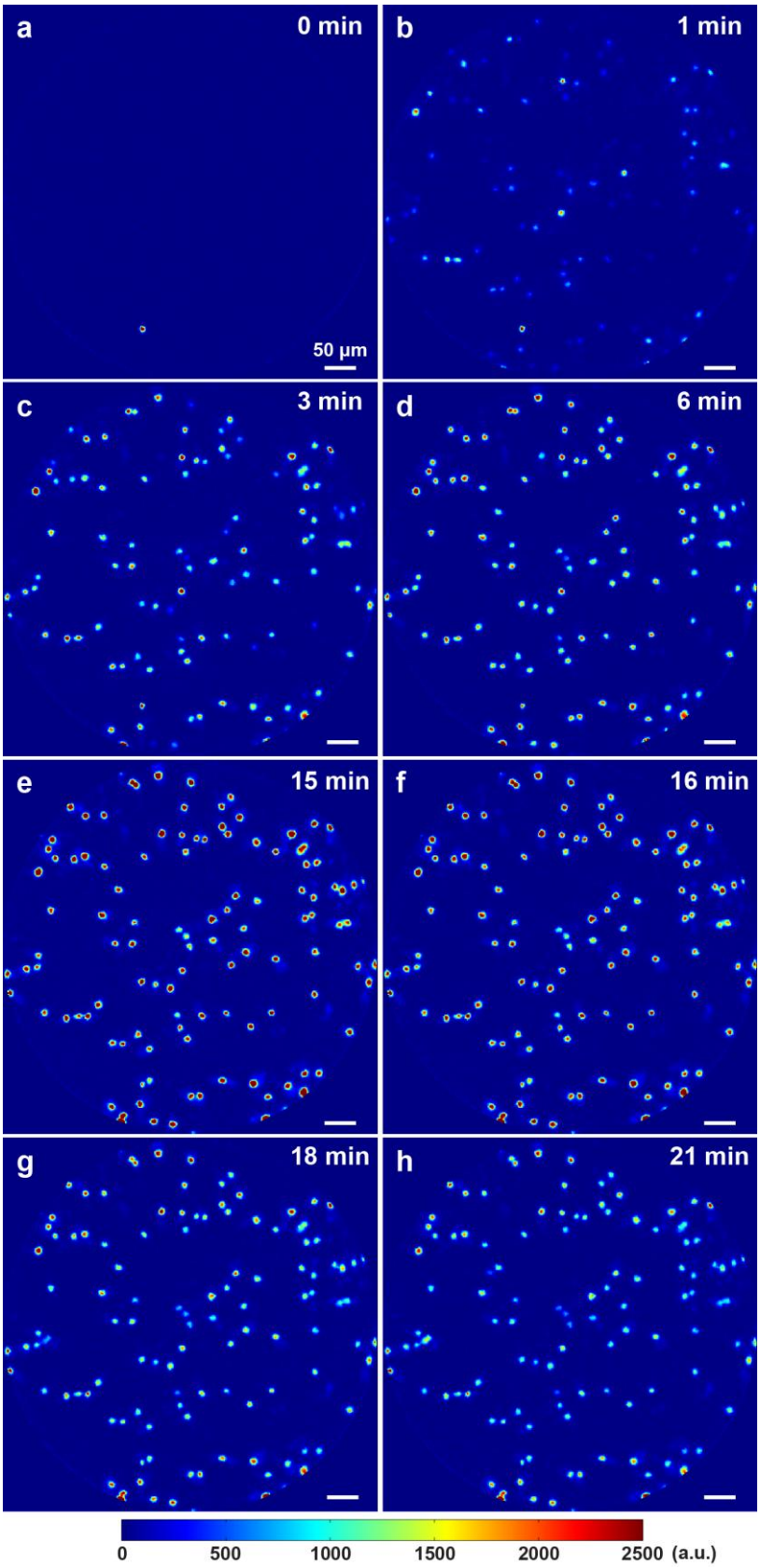

Figure 2. Snapshots of a representative monitoring of the US- and microbubble-mediated SYTOX Green uptake (a-d), and the subsequent sequence collected for PB evaluation (e-h). The cell monolayer

is not exposed to excitation light from 6 minutes to 15 minutes, preventing PB during this interval. Bar = 50 µm.

Using the PB model (Eq. 2), the PB rates collected cell-by-cell significantly increased (MW, $p < 0.05$) as a function of the laser power: 1.0 10^{-3} s^{-1} (0.4 10^{-3} s^{-1}), 2.1 10^{-3} s^{-1} (0.7 10^{-3} s^{-1}) and 2.9 10^{-3} s^{-1} (0.9 10^{-3} s^{-1}) at 25 %, 50 % and 75 % of laser power, respectively, indicating a clear impact of the laser power on SYTOX Green PB (figure 3).

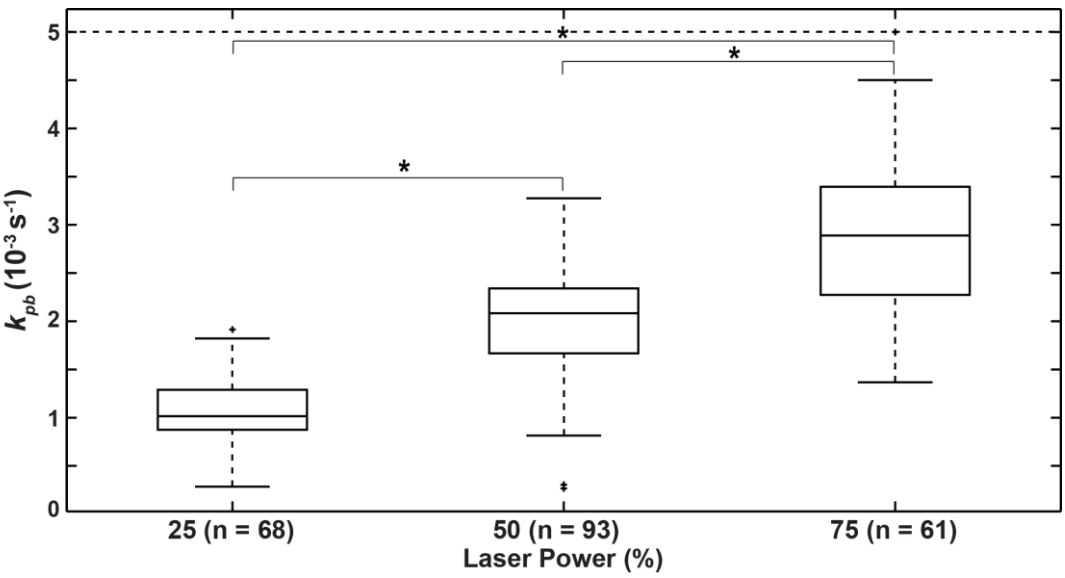

Figure 3. Experimental evaluation of PB rates cell-by-cell (*$p < 0.05$). The photobleaching rate collected experimentally increases when the laser power increases.

Sensitivity of the Three-compartment Model and Influence of the Acquisition Time

In the range of uptake rates and PB rates obtained experimentally using the $3CM_{ref}$ (Eq. 3), the sensitivity of the three-compartment model was evaluated for 3 time windows. The normalized errors of $\hat{k}_{up}$ were small, and showed no clear dependence on the true values of k_{up} and k_{pb}. The maximum normalized error found was 0.6 %, 0.2 % and 0.2 % for acquisitions of 3 minutes, 6 minutes and 9 minutes, respectively, indicating that for uptake rates in our experiments it is beneficial to acquire data for at least 6 min, but that the normalized error is not lowered when the acquisition time is further to 9 min (figure 4a,c,e).

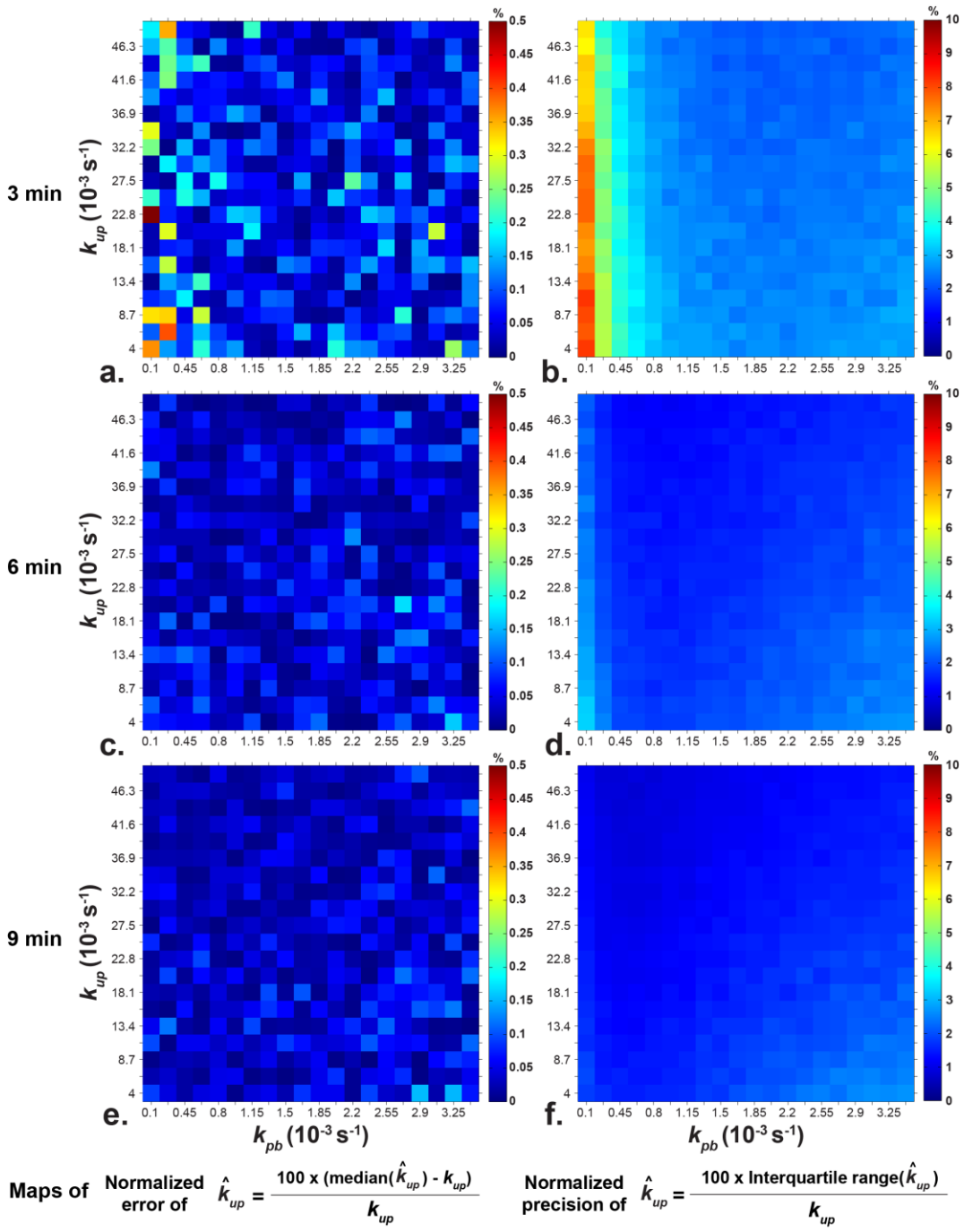

Figure 4. Sensitivity maps of the three-compartment model. a.c.e. Normalized error with a 3 (a), 6 (c) and 9 minute (e) acquisition. b.d.f. Normalized precision with a 3 (b), 6 (d) and 9 minute (f) acquisition.

The precision of $\hat{k}_{up}$ was better than 8.2 %, 3.3 % and 2.7 %, for all simulated k_{up} and k_{pb} (figure 4b,d,f), for acquisition windows of 3 minutes, 6 minutes and 9 minutes, respectively. For the short acquisition window, the variability in the estimated uptake rates was notably higher for low

uptake rates, and the more so when PB rate was low. In addition, for all observation durations, variability increased for combinations of high PB rate and low uptake rate, *i.e.* when $k_{up} \approx k_{pb}$. If, for our purposes in our experiment, a precision of 5 % is regarded as satisfactory, it is thus sufficient to acquire data using a 6-minute time window.

Comparison of the methods

After the uptake and PB profiles for individual cells were extracted from the data, results from the 2CM and the $3CM_{all}$ methods were compared to the $3CM_{ref}$ method, which is our reference method in this study (see section "Real-Time Imaging of Model Drug Uptake and Experimental Evaluation of Photobleaching") (figure 5a-c).

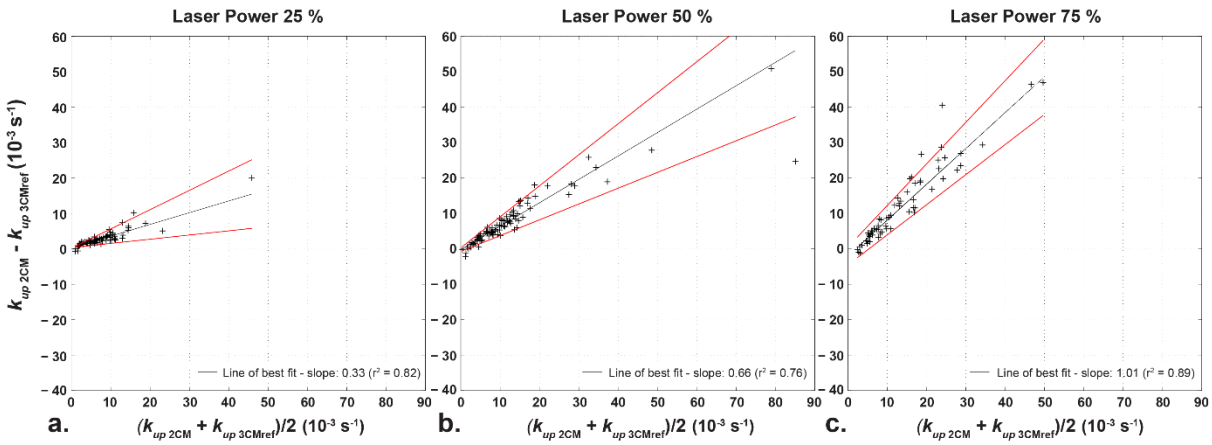

Figure 5. Bland-Altman plots of the uptake rate estimates using the 2CM compared to the $3CM_{ref}$ at 25 % (a), 50 % (b) and 75 % (c) of laser power. The scatter plots show a proportional bias with heteroscedasticity.

The Bland-Altman plot indicates a proportional bias with an increasing overestimation of the uptake rate by the 2CM when the average value increases. The overestimation increased with laser power and the PB induced, as shown by the stronger slope of the line of best fit: 0.33, 0.66 and 1.01 at 25 %, 50 % and 75 % of laser power, respectively (figure 5a-c, dark line). In addition, the scattergram

expands when the average value increases, which is characteristic of heteroscedasticity. This spread increases linearly when the uptake rate increases (figure 5a-c, red lines).

For the majority of the points in the low range 0 - 10 10^{-3} s^{-1}, comparison of the $3CM_{all}$ with the $3CM_{ref}$ indicates a proportional bias with a negative slope, indicating that the $3CM_{all}$ underestimates the uptake rate (figure S1a-c). For the other data points with an average uptake rate larger than 10.0 10^{-3} s^{-1}, no clear trend can be identified. Considering all the points, difference values display an average of -1.7 10^{-3} s^{-1}, -0.5 10^{-3} s^{-1}, and 2.8 10^{-3} s^{-1} at 25 %, 50 % and 75 % of laser power, respectively (figure S1a-c, black horizontal line).

Distribution of Pharmacokinetic Parameters

First, the uptake rates calculated by the $3CM_{ref}$ at 25 %, 50 % and 75 % of laser power were in agreement (MW, $p > 0.05$), indicating that the 3-compartment model allowed assessing the uptake rates of the cells irrespective of the amount of PB (figure 6a-c and Table S1).

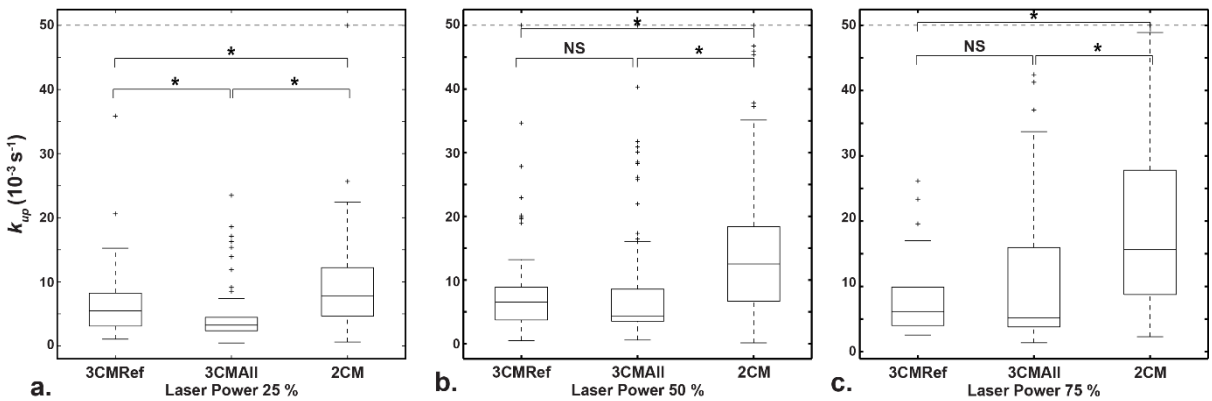

Figure 6. Box plots of the uptake rates obtained with the $3CM_{ref}$, the $3CM_{all}$ and the 2CM at 25 % (a), 50 % (b) and 75 % (c) of laser power. *$p < 0.05$. Non-significant differences (NS): $p > 0.05$.

Conversely, the 2CM that was commonly used before this study showed significant differences (MW, $*p < 0.05$) in the uptake rates obtained at different laser powers. The median values doubled and the interquartile ranges increased by a factor of 2.5 from 25 % to 75 % of laser power, *i.e.* with a stronger PB (figure 6a-c), suggesting a limited accuracy of the 2CM.

With the $3CM_{all}$, which is based on the 3-compartment model (Eq. 3) and does not have experimentally obtained independent knowledge on the PB rate, the uptake rate estimates at 25 % of laser power, were significantly lower than those at 50 % (MW, $*p < 0.05$), however, no difference was observed in the uptake rate estimates between 50 % and 75 % of laser power (figure 6a-c and Table S1). As also observed for the 2CM, the interquartile range increases when the PB is higher. Moreover, a significant difference is observed between the $3CM_{ref}$ and the $3CM_{all}$ at 25 % of laser power (WX, $*p < 0.05$) (figure 6a), but similar uptake rate estimates were found with the $3CM_{all}$ compared to the $3CM_{ref}$ (WX, $p > 0.05$) at 50 % and 75 % of laser power (figure 6b-c and Table S1). This suggests that the $3CM_{all}$ becomes more robust when exciting the fluorophores with a significant laser power. If we then compare the PB rates obtained by the $3CM_{all}$ with those obtained in a separate PB measurement as used in $3CM_{ref}$, similar estimates (WX, $p > 0.05$), were found only at 75 % of laser power, again indicating that the PB must be high enough to be sensed in the fitting procedure (figure S2a-c).

Discussion

PB is a frequently occurring problem in applications of intensity-based dynamic fluorescence microscopy [25]. For instance, in single-particle tracking applications, signal-intensity based detection of single particles is hindered by PB [26], thus requiring its evaluation and methods to compensate for it. PB compensation is all the more important when the quantity of interest is directly derived from fluorescence signal intensity. In our specific application, PB had an impact on pharmacokinetic parameter estimates collected in US- and microbubble-mediated plasma membrane permeabilization using FCFM *in vitro*. A previous study proposed a two-compartment model to describe the cell uptake of SYTOX Green model drug triggered by US and microbubbles [18]; to model the irreversible

destruction of fluorophores by PB, a third compartment taking up the fluorophores bound to DNA was added, and it was demonstrated that incorporating PB led to more consistent results, independent of the applied laser power. In the context of US- and microbubble-mediated drug delivery, this study is the first to analyze systematically PB impact and compensate for it on the uptake kinetic parameter estimates of a model drug measured by dynamic confocal fluorescence microscopy.

After the acquisition of the uptake profile and after the SYTOX Green fluorescence signal had further equilibrated, the collection of the PB profile in each individual cell was performed in the same field of view, ensuring the same optical path. The PB rates were measured larger when the laser power increased, but overall lower than 5.0 10^{-3} s^{-1}. In addition, the heterogeneity of the PB rate distribution increased with a greater laser power. In the scope of this study, for the sake of stability of the fit and according to the PB profiles, a mono-exponential model was chosen.

Using simulations, the numerical stability of the uptake rate estimates to wrong estimations of the PB rate was found to be low. We showed that it is advantageous to set the observation window of the imaging protocol at least twice the characteristic time constant, especially when both k_{up} and k_{pb} are fitted from this data simultaneously.

The 2CM and the $3CM_{all}$ were compared to the $3CM_{ref}$, which integrates independent knowledge by means of an experimental PB rate. The latter was the reference method of this study. We observed that the 2CM introduces a bias, that is, linearly proportional to the uptake rate, *i.e.* the larger the uptake rates in a cell population, the higher their overestimation by the 2CM. This overestimation is also observed in the synthetic data exemplified in Figure S3, and can be explained by the inability for the 2CM to fit adequately the local maximum in the fluorescence signal profile, that is introduced by PB. Therefore, the least-squares fit based on the 2CM solves the minimization problem by overestimating the uptake rate. It should also be noted that this overestimation is even larger when the PB is higher, as reflected by the slope of the proportional bias as a function of laser power. These observations indicated that PB has an impact on the uptake rate estimates, and must be taken into account to compensate for it. Finally, the methods were compared for their potential to

accurately assess uptake rate in a cell population. Using PB rates from a separate measurement phase, $3CM_{ref}$ found uptake rates irrespective of the laser power applied, which demonstrates adequate PB correction for this three-compartment model. To investigate if it would be possible to obtain uptake and photobleaching rate from a single acquisition window, we compared the $3CM_{all}$, in which all parameters are free in the fit procedure, to the $3CM_{ref}$. The Bland-Altman plot did not indicate a clear trend, but an increasing underestimation is noticeable for uptake rate estimates below 10.0 10^{-3} s^{-1} for the 3 laser powers. The cause of this underestimation and the range where it is applicable remain unclear, but at 25 % and 50 % of laser power, this underestimation of the uptake rates using the $3CM_{all}$ is associated with an overestimation of the PB rates compared to those found using the $3CM_{ref}$. In addition, the scattergrams for each of the laser powers showed no pattern for uptake rates greater than 10.0 10^{-3} s^{-1}.

When PB and uptake are fitted simultaneously from a time series, it is necessary to perform a pilot experiment and, from the resulting time constants, set the time of acquisition so the sequence is long enough and the PB rate must be high enough, but in a range of laser power where no heat is generated, to have substantial effect in the last part of the sequence and thus be adequately sensed by the $3CM_{all}$ model. This finding helps us to design future imaging protocols related to this application. Interestingly, this runs counter to the common instruction in fluorescence microscopy advising to set the intensity of the excitation light as low as possible to limit PB.

Conclusion

This study established a methodology to evaluate PB, investigate its impact on kinetic parameter estimates measured by dynamic fluorescence microscopy, and compensate for PB using a three-compartment model. It was demonstrated that a 3CM model helped to improve the accuracy of the uptake pharmacokinetic parameter estimates in a cell population subjected to microbubble-assisted sonopermeabilization by US waves.

Acknowledgments

This study was funded by the ERC project 268906 "Sound Pharma" (Prof. C. Moonen). The authors thank Dr. Sébastien Benzekry (IMB, UMR 5251, CNRS, Université de Bordeaux, Bordeaux, France) for the fruitful discussion on the theoretical robustness of the 3-compartment model.

References

[1] Allen T M and Cullis P R 2004 Drug delivery systems: entering the mainstream *Science* **303**(5665) 1818–1822

[2] Yeh E T H 2004 Cardiovascular Complications of Cancer Therapy: Diagnosis, Pathogenesis, and Management *Circulation* **109** 3122–3131.

[3] Skauen D M and Zentner G M 1984 Phonophoresis *Int J Pharm* **20**(3):235–245

[4] Miller M W, Miller D L and Brayman A A 1996 A review of in vitro bioeffects of inertial ultrasonic cavitation from a mechanistic perspective *Ultrasound Med Biol* **22**(9) 1131–1154

[5] Mitragotri S 2005 Healing sound: the use of ultrasound in drug delivery and other therapeutic applications *Nat Rev Drug Discov* **4**(3) 255–260

[6] Ter Haar G 2007 Therapeutic applications of ultrasound *Prog Biophys Mol Biol* **93**(1–3) 111–129

[7] Ter Haar G 2012 Ultrasound mediated drug delivery: A 21st century phoenix? *Int J Hyperthermia* **28**(4) 279–281

[8] Deckers R, Yudina A, Cardoit L C and Moonen C 2011 A fluorescent chromophore TOTO-3 as a 'smart probe' for the assessment of ultrasound-mediated local drug delivery in vivo *Contrast Media Mol Imaging* **6**(4) 267–274

[9] Fricker M, Runions J and Moore I 2006 Quantitative Fluorescence Microscopy: From Art to Science *Annu Rev Plant Biol* **57**(1) 79–107

[10] Muzzey D and van Oudenaarden A 2009 Quantitative Time-Lapse Fluorescence Microscopy in Single Cells *Annu Rev Cell Dev Biol* **25** 301–327

[11] Stepanova T, Slemmer J, Hoogenraad C C, Lansbergen G, Dortland B, de Zeeuw C I, Grosveld F, van Cappellen G, Akhmanova A and Galjart N 2003 Visualization of Microtubule Growth in

Cultured Neurons via the Use of EB3-GFP (End-Binding Protein 3-Green Fluorescent Protein) *J Neurosci* **23**(7) 2655–2664

[12] Jaqaman K, Loerke D, Mettlen M, Kuwata H, Grinstein S, Schmid S L and Danuser G 2008 Robust single-particle tracking in live-cell time-lapse sequences *Nat. Methods* **5**(8) 695–702

[13] Rosenthal E and Zinn KR 2009 *Optical Imaging of Cancer: Clinical Applications* Springer

[14] Song L, Hennink E J, Young I T and Tanke H J 1995 Photobleaching kinetics of fluorescein in quantitative fluorescence microscopy *Biophys J* **68**(6) 2588–2600

[15] Benson D M, Bryan J, Plant A L, Gotto A M and Smith L C 1985 Digital imaging fluorescence microscopy: spatial heterogeneity of photobleaching rate constants in individual cells *J Cell Biol* **100**(4) 1309–1323

[16] Rigaut J P and Vassy J 1991 High-resolution three-dimensional images from confocal scanning laser microscopy. Quantitative study and mathematical correction of the effects from bleaching and fluorescence attenuation in depth *Anal Quant Cytol Histol/Int Acad Cytol Am Soc Cytol* **13**(4) 223–232

[17] Smal I, Niessen W and Meijering E 2007 Advanced particle filtering for multiple object tracking in dynamic fluorescence microscopy images *4th IEEE International Symposium on Biomedical Imaging: From Nano to Macro* 1048–1051

[18] Derieppe M, Yudina A, Lepetit-Coiffé M, Denis de Senneville B, Bos C and Moonen C 2013 Real-Time Assessment of Ultrasound-Mediated Drug Delivery Using Fibered Confocal Fluorescence Microscopy *Mol Imaging Biol* **15**(1) 3–11

[19] Derieppe M, Denis de Senneville B, Kuijf H, Moonen C and Bos C 2014 Tracking of Cell Nuclei for Assessment of In Vitro Uptake Kinetics in Ultrasound-Mediated Drug Delivery Using Fibered Confocal Fluorescence Microscopy *Mol Imaging Biol* **16**(5) 642–651

[20] Cressie N A C 1993 *Statistics for Spatial Data* Wiley-Interscience Revised Edition

[21] Song L, van Gijlswijk R P M, Young I T and Tanke H J 1997 Influence of fluorochrome labeling density on the photobleaching kinetics of fluorescein in microscopy *Cytometry* **27**(3) 213–223

[22] Bland J M and Altman D G 1986 Statistical methods for assessing agreement between two methods of clinical measurement *The Lancet* **327**(8476) 307–310

[23] Bland J M and Altman D G 1999 Measuring agreement in method comparison studies *Stat Methods Med Res* **8**(2) 135–160

[24] Ludbrook J 2010 Confidence in Altman–Bland plots: A critical review of the method of differences *Clin Exp Pharmacol Physiol* **37**(2) 143–149

[25] Vicente N B, Zamboni J E D, Adur J F, Paravani E V and Casco V H 2007 Photobleaching correction in fluorescence microscopy images *J Phys Conf Ser* **90**(1) 012068

[26] Smal I, Draegestein K, Galjart N, Niessen W and Meijering E 2008 Particle filtering for multiple object tracking in dynamic fluorescence microscopy images: Application to microtubule growth analysis *IEEE Trans Med Imaging* **27**(6) 789–804

Supplementary data

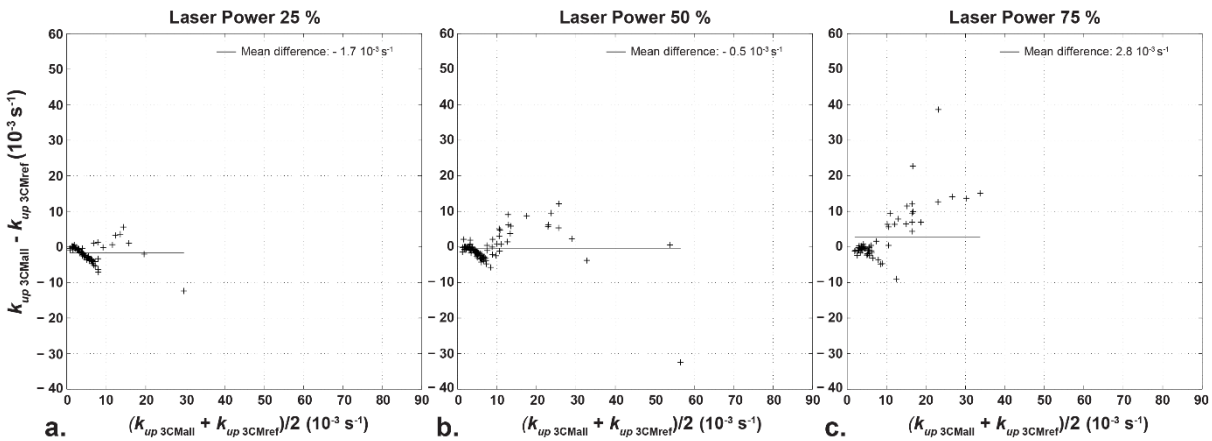

Figure S1. Bland-Altman plots of the uptake rate estimates using the $3CM_{all}$ compared to the $3CM_{ref}$ at 25 % (a), 50 % (b) and 75 % (c) of laser power.

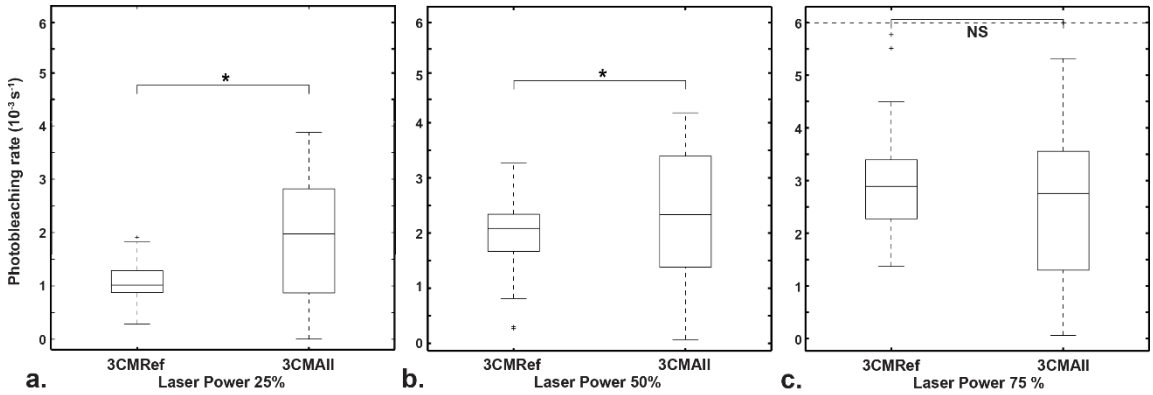

Figure S2. Box plots of the photobleaching rates obtained with the $3CM_{ref}$ and the $3CM_{all}$ at 25 % (a), 50 % (b) and 75 % (c) of laser power. *$p < 0.05$. Non-significant differences - NS: $p > 0.05$.

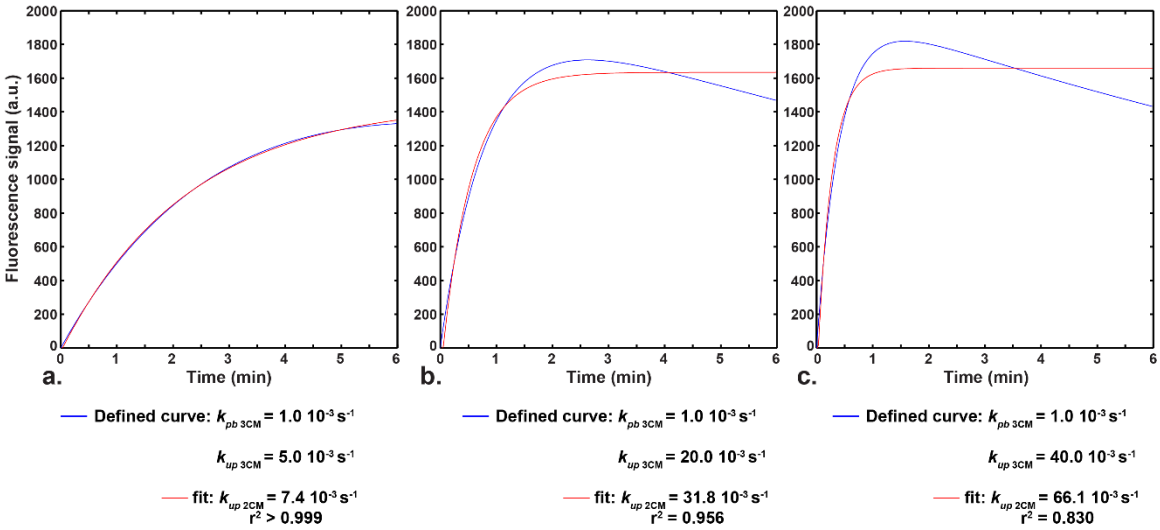

Figure S3. Examples of uptake rates obtained with the 2CM from synthetic signal profiles generated with 5.0 10^{-3} s^{-1} (a), 20.0 10^{-3} s^{-1} (b) and 40.0 10^{-3} s^{-1} (c) of uptake rates, a photobleaching rate of 1.0 10^{-3} s^{-1} (corresponding to 25% of laser power), and an asymptote of 2000 a.u. applied in each case.

Table S1. Table of the uptake rate estimates obtained with the methods $3CM_{ref}$, 2CM and $3CM_{all}$. median (interquartile range).

Uptake rates (10^{-3} s^{-1})		**Method**		
		$3CM_{ref}$	**2CM**	**$3CM_{all}$**
Laser Power	**25 %**	**5.5 (5.1)**	**7.8 (7.6)**	**3.2 (2.1)**
	50 %	**6.5 (5.1)**	**12.5 (11.7)**	**4.3 (5.0)**
	75 %	**6.1 (5.9)**	**15.6 (19.0)**	**5.2 (12.1)**

Table S2. Table of the photobleaching rate estimates obtained with the methods $3CM_{ref}$ and $3CM_{all}$. median (interquartile range).

Photobleaching rates (10^{-3} s^{-1})		**Method**	
		$3CM_{ref}$	**$3CM_{all}$**
Laser Power	**25 %**	**1.0 (0.4)**	**2.0 (1.9)**
	50 %	**2.1 (0.7)**	**2.3 (2.0)**
	75 %	**2.9 (0.9)**	**2.8 (2.2)**